

EFFECT OF SILICON AND MICROSTRUCTURE ON SPHEROIDAL GRAPHITE CAST IRON THERMAL CONDUCTIVITY AT ELEVATED TEMPERATURES

Kalle Jalava , Kaisu Soivio, and Juhani Orkas

Department of Mechanical Engineering, Aalto University, Otakaari 4, 00076 Aalto, Finland

Jarkko Laine

Wärtsilä Finland Oy, Järvikatu 2-4, 65100 Vaasa, Finland

Copyright © 2017 American Foundry Society
DOI 10.1007/s40962-017-0184-1

Abstract

Spheroidal graphite cast irons are materials that exhibit many possible microstructures and compositions, which in turn create a multitude of possible property combinations. Chemical composition and microstructure are some of the biggest influences on these material properties. This paper concentrates on the effect of silicon alloying in the range of 1–4% and varying ferrite–pearlite microstructures on thermal conductivity of spheroidal graphite cast irons from room temperature up to 400 °C. Results show that increasing silicon alloying levels decreases thermal conductivity, while a decreasing trend is also seen with increasing pearlite fraction, as composition and

morphology act as hindrance to thermal conduction. Temperature dependence shows as an initial increase in thermal conductivity and a peak near 200–300 °C for the studied alloys. Based on the results, a model estimating thermal conductivity with silicon alloying, pearlite fraction and temperature is made to aid in the estimation of material properties for design use.

Keywords: cast iron, ductile iron, spheroidal graphite, thermal conductivity, elevated temperatures

Introduction

Cast irons are essentially composite structures, including graphite in various morphologies, and are widely used in applications that combine the need for good thermal transport and mechanical properties. Multiple positive effects arise from the graphite in their microstructures, ranging from vibrational damping to thermal transport. Microstructural differences due to a multitude of production steps and possible part geometries necessitate gaining more knowledge of corresponding properties. Regarding design of complex thermally stressed components, like those in internal combustion engines, all too little is currently known in detail how different material parameters affect elevated temperature behavior of cast irons. Trends in component design have also increasingly shifted from

using assumptions of a mostly homogenous material behavior to a localized property approach.^{1–3} Profound understanding and data of materials are needed for any computational approach to be usable and accurate.

Design data of mechanical properties are available in abundance compared to detailed thermal properties, which naturally complicates the design of thermally stressed components and forces one to make assumptions about unknown parameters. Some data are available from literature, but often notations of important parameters such as microstructural composition are somewhat ambiguous. Generally, thermal conduction in metals is due to electron and phonon contribution to heat propagation. Both mechanisms of heat propagation are lessened by obstacles in lattice; for example, inclusions, impurities, alloying elements, dislocations.⁴ Specifically, with cast irons, thermal properties are mainly influenced by chemical composition,^{5–8} or alloying, graphite morphology^{8–13} and microstructure.^{14–16} Most of those connect to each other in

Electronic supplementary material The online version of this article (doi:10.1007/s40962-017-0184-1) contains supplementary material, which is available to authorized users.

actual production processes. Mechanical properties also have variations through these parameters, but unfortunately often inversely to thermal properties. Spheroidal graphite cast iron generally have the best mechanical properties in the larger group of cast irons. On the other hand, there is almost no additional thermal benefit from nodular graphite.^{9,17} These differing effects have been attributed to come from graphite conducting heat optimally through specific basal planes,¹⁷ which for spheroidal graphite has somewhat negligible difference compared to similarly alloyed (matrix alloying levels) cast steels. Gray and compacted graphite alloys' thermal property optimization is often done through graphite control, while in contrast the nature of spheroidal graphite forces one to focus more on microstructural and compositional control.

Heat treatments and controlled cooling systems are widely used to change material microstructures to improve and tune mechanical properties. For cast irons, heat treatments can be used to control ferrite and pearlite ratios or change the microstructure entirely, e.g., austempering treatments (ADI). Ferrite is a much better thermal conductor than pearlite,⁴ but results in lower strength, if not solution-strengthened with proper alloying elements. Higher alloying levels, for example high silicon in relatively newly standardized solution-strengthened ferritic ductile irons (SSF), give better mechanical properties combined with a homogenous ferritic microstructure,^{18–20} but will have more disruptive effects to thermal transport properties compared to low alloy ferrite. Changes in microstructure also naturally arise from cast part geometries, like wall thicknesses. A part might also have a multitude of ferrite and pearlite compositions in the geometry due to different internal cooling rates alone. This heterogeneity can be a challenge or a possibility for design engineers. In the end, proper material data are of utmost importance especially in simulation and general design of components.

The aim of this work was to study thermal properties of spheroidal graphite cast iron with different variations in silicon alloying levels, along with a multitude of ferrite–pearlite microstructural compositions through heat treatments. The work consists of heat treatments, microstructural analysis and subsequent thermal property measurements of spheroidal graphite alloys with differing silicon alloying levels. The obtained experimental data were further analyzed through statistical regression, and the resulting model is tested with two additional as-cast alloys.

Experimental Procedure

Studied compositions shown in Table 1 cover the standard alloying ranges for spheroidal graphite cast iron. Alloy 1 is near the easily attainable lower limit of silicon alloying as some silicon is in most cases introduced to a melt from important metallurgical treatments like spheroidizing and

Table 1. Chemical Compositions of Studied Alloys (w-%) and Some Nearest Corresponding Grades According to Standard EN 1563

Alloy	C	Si	Mn	P	S	CE %	Note
1	4.0	1.5	0.1	0.02	0.004	4.5	Low silicon
2	3.6	2.3	0.5	0.03	0.015	4.4	GJS 500-7
3	3.4	3.8	0.4	0.03	0.008	4.7	GJS 500-14
4	2.8	4.3	0.3	0.02	0.003	4.2	GJS 600-10

inoculation. Carburizing a low alloy melt also becomes increasingly difficult when trying to offset the decrease in carbon equivalent (CE%). Alloy 2 is an intermediate composition, which corresponds to a common ferritic–pearlitic variant in the standard EN 1563, namely EN GJS 500-7. Alloy 3 is a solution-strengthened composition in the higher range of silicon alloying, corresponding to EN GJS 500-14 standard and alloy 4 a bit higher still in silicon alloying, corresponding to EN GJS 600-10. All the samples in this study were cut from separately cast, roughly 25-mm-diameter tensile test bar blanks.

Samples from the four tested alloys were heat-treated in order to vary microstructure, in this case ferrite–pearlite ratios. Heat treatments consisted of austenization for 2 h at 900 °C for alloys 1 and 2, and 2 h at 950 °C for alloys 3 and 4 due to their different silicon levels. These were followed with either slow furnace cooling to facilitate ferritic microstructures, faster natural air cooling for the most pearlitic variants or intermediate steps at 680–700 °C for various times followed by air cooling to get varying amounts of pearlite in the microstructure.

Microstructural image analysis was used after heat treatment to calculate ferrite–pearlite fractions and to check for possible unwanted changes in graphite morphology. Samples were ground and polished, graphite fraction analyzed from images of unetched samples and absolute ferrite–pearlite area fractions from Nital-etched samples like the ones shown in Figure 1. Thus, for clarity it should be noted that a fully pearlitic microstructure would be less than 100% pearlite in the results as some area is always occupied by nodular graphite particles.

Hot Disk TPS 2500 S thermal constants analyzer based on ‘Transient Plane Source’ (TPS) method, capable of measuring high thermal conductivities of metals like copper and aluminum alloys,^{21–24} was used to measure thermal conductivities of the alloys from room temperature up to 400 °C. Room temperature measurements were made in stainless steel sample holders with a Kapton insulated sensor. Elevated temperature tests were made with an automatically controlled muffle furnace, which contained a high-temperature sample holder with Mica insulated

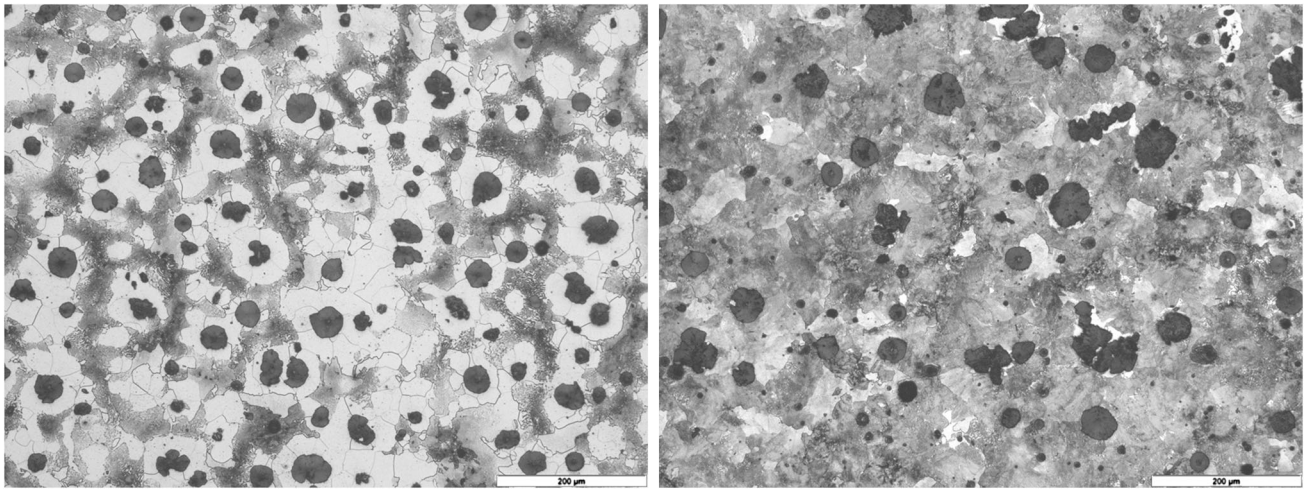


Figure 1. Example microstructures used in characterization, alloy 2 at 41% pearlite abs. (left) and 92% abs. (right).

sensors. Test samples were stabilized at selected temperatures for at least 30 min before conducting measurements to lessen the effect of temperature drift and other variation sources in thermal property calculations. Elevated temperature tests consisted of a single cycle that went in steps from lower temperatures to higher. The used cylindrical samples illustrated in Figure 2 were cut from the cast tensile test bar blanks after heat treatment.

In the Hot Disk TPS method, a transient plane source sensor is placed between the surfaces of one or two pieces of sample(s) to be measured, shown in Figure 2. During measurement, current passes through a nickel spiral in the sensor, which creates an increase in temperature. The heat generated in the sensor flows through the sample at a rate dependent on thermal transport characteristics of the studied material. Heat propagated needs to be confined within the sample boundaries or be insulated properly and be of known dimensions, and thus, in property calculations it can be assumed as infinite, bulk material. By recording

the temperature versus time response in the sensor, thermal transport characteristics including thermal conductivity can be calculated. The method has been shown to be useful for measuring engineering materials with high thermal conductivity.²¹⁻²⁴ Represented in a very simplified manner, thermal properties can be identified from a single transient measurement using the following equations:

$$\lambda = \kappa \rho c \quad \text{Eqn. 1}$$

$$\tau = \frac{\sqrt{\kappa t}}{a} \quad \text{Eqn. 2}$$

where λ is thermal conductivity, κ thermal diffusivity, ρ density, c specific heat and τ a dimensionless parameter called characteristics time, including time t and sensor radius a . Thermal property values are calculated from slope of a complex time function $D(\tau)$ and average temperature increase $\Delta \bar{T}(\tau)$ plot. As many of the parameters are not known beforehand, measurement software is used to optimize a solution until a linear fit is achieved. This ultimately makes it possible to measure a property like thermal conductivity without measuring specific heat independently. In depth, theoretical background of a 'hot disk' measurement is presented in referenced material.²³

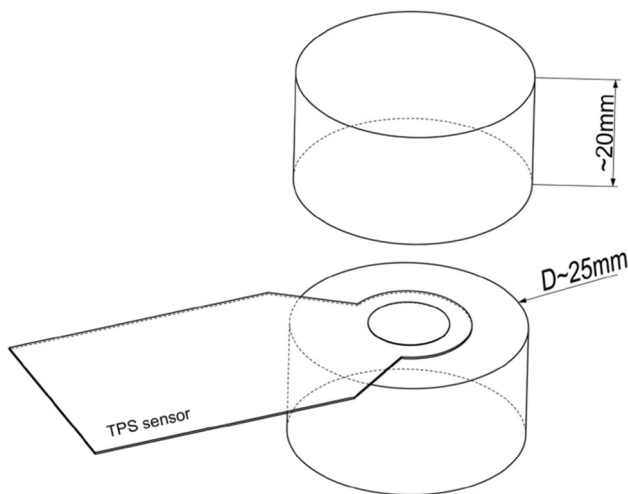


Figure 2. Representation of a transient plane source sample setup used in this study.

Results

Compiled measured thermal conductivities and microstructural compositions are presented in Figure 3. Temperature, silicon and pearlite have clear effects on resulting final thermal conductivity. The low silicon alloy 1 shows the best elevated temperature thermal properties of the studied materials with thermal conductivity of 59 W/mK at around 200 °C with a mostly ferritic microstructure. On the other hand, the highest alloyed alloy 4 has the lowest conductivity results with high amounts of pearlite in the microstructure. Generally, with all the tested alloys, an increase in thermal conductivity can be seen with rising temperature until a peak is attained, but a clear decrease is seen with increase in silicon alloying levels and pearlite

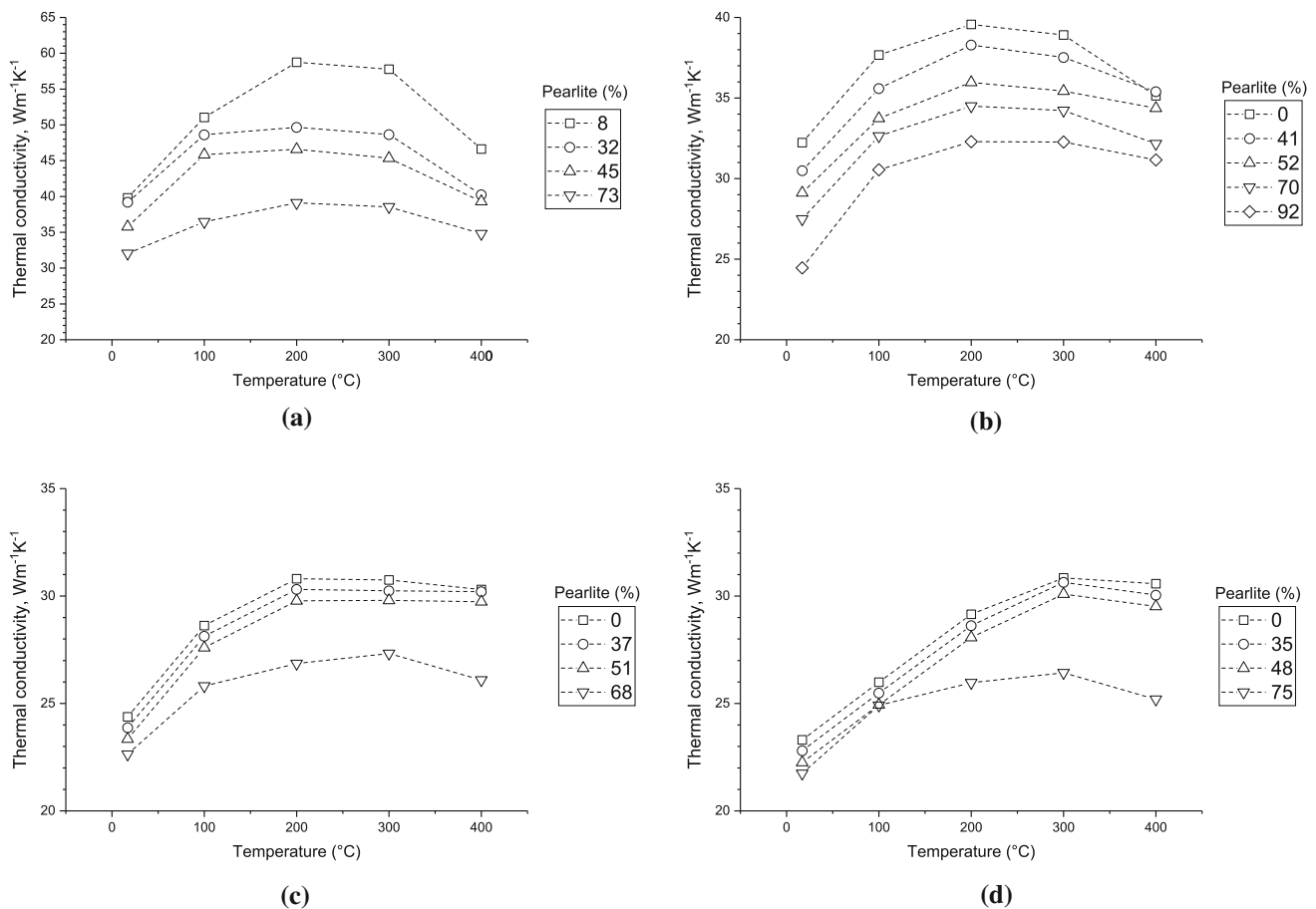


Figure 3. Thermal conductivities of (a) alloy 1, 1.5% Si, (b) alloy 2, 2.3% Si, (c) alloy 3, 3.8 Si %, (d) alloy 4, 4.3% Si with different ferrite–pearlite ratios.

fraction. The results show that the studied parameters have big influences on final thermal properties of spheroidal graphite cast iron.

The results shown in Figure 3 were used to make a multi-parameter regression model in Minitab—statistical analysis software. Regression resulted in the following equation.

$$\lambda \left(\frac{W}{mK} \right) = 72.56 + 0.06721x_1 - 21.67x_2 - 0.2458x_3 - 0.000161x_1^2 + 2.173x_2^2 + 0.00414x_1x_2 + 0.0541x_2x_3, \quad \text{Eqn. 3}$$

where x_1 = temperature (°C), x_2 = silicon (%) and x_3 = pearlite (% abs.) $R^2 = 0.92$ $P < 0.001$.

The regression model was tested with two additional as-cast spheroidal graphite alloys out of the original data put into modeling. These test alloys had slightly different silicon levels, but varied mostly in pearlite content controlled by copper additions. Comparison between the model and measured values for these additional alloys are shown in Figure 4 and the additional alloys' chemical compositions

(w-%) in Table 2. Estimated values from the model matched quite closely to actual measured values.

Discussion

Increasing silicon alloying decreases thermal conductivities with all microstructures. Even in a fully ferritic state, measured thermal conductivity of alloy 4 is far from alloy 1. High amounts of silicon in solid solution have many benefits for cast iron mechanical properties,^{18–20} but is clearly not beneficial for thermal properties. Thus, tuning chemical compositions for better mechanical properties through solution strengthening will worsen thermal properties and vice versa. However, the general effect of silicon on thermal conductivity is not linear, as shown in the main effect plots in Figure 5 calculated from the aggregate data. The decrease in conductivity is initially rapid in the low silicon ranges, while increasing alloying has a clear saturating behavior showing as a change in the slope at around ~ 3–4% silicon. Similar kind of saturating behavior can be seen in mechanical behavior, as increasing silicon alloying to over 4.3% has been shown to deteriorate properties like elongation in solution-strengthened spheroidal graphite cast irons²⁰ making them unusable for

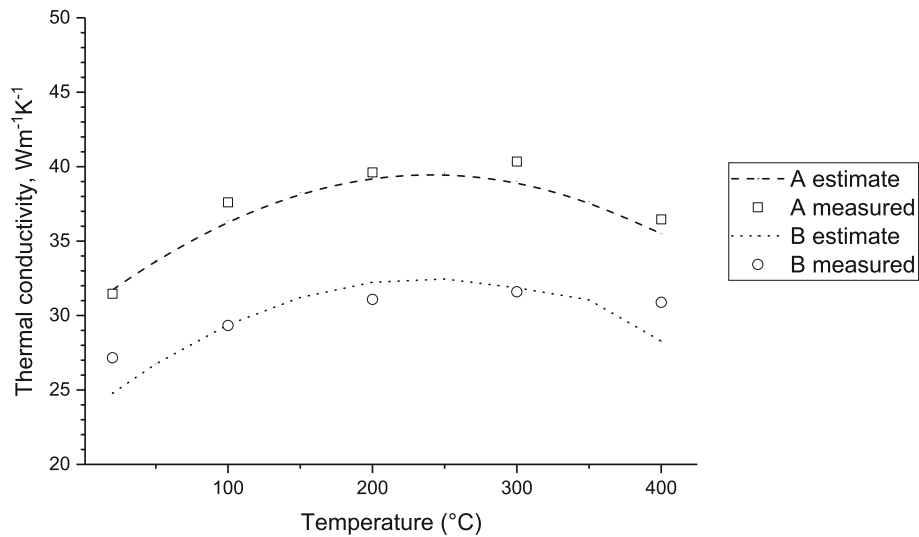


Figure 4. Comparison between estimates of Eqn. 3 and measured values for test alloys A (upper) and B (lower).

Table 2. Chemical and Microstructural Composition of Alloys Used to Test Eqn. 3

Alloy	C	Si	Mn	P	S	Cu	CE %	Pearlite (%)	Note
A	3.7	2.5	0.4	0.03	0.009	0.1	4.5	15	GJS 400-15
B	3.6	2.3	0.4	0.03	0.009	0.4	4.4	88	GJS 600-3

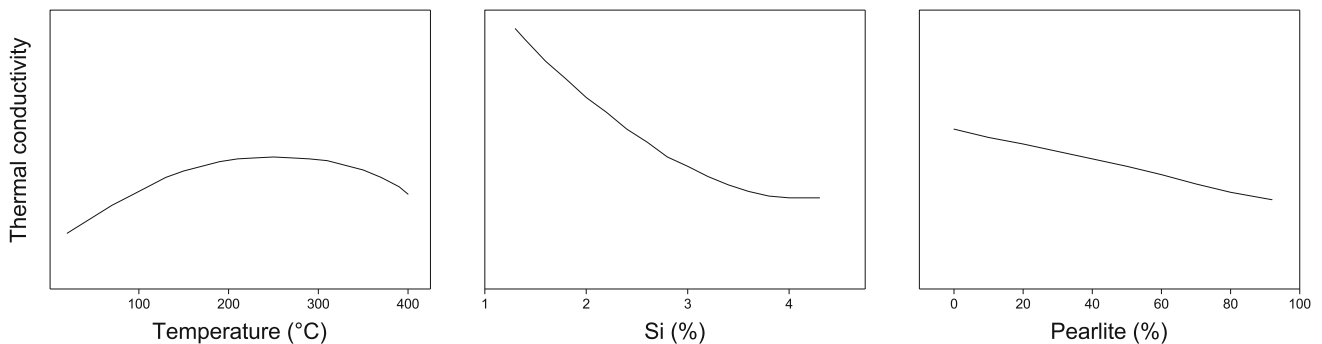


Figure 5. Main effect plots of studied parameters: temperature, silicon and pearlite used in regression modeling.

structural use after the silicon embrittlement range has been reached.

The general shape of the elevated temperature curve shown in Figure 5 is consistent for all the tested alloys and microstructures. The results indicate that the temperature dependence is not linear in nature, seen as some initial increase toward higher temperatures, which peaks at around 200–300 °C, and with a final decrease toward higher temperatures. Generally, for all the tested alloys, the main effect plot shows a peak at 250 °C. Test alloy 4 peaks at a slightly higher temperature than the others do, which is not truly surprising as it is farthest from being a pure material, containing the most hindrances to conduction in

terms of silicon alloying combined with pearlite. The temperature effect happens with all microstructures from ferritic to pearlitic along with all tested silicon alloying levels, which indicates that it is not only a property of a specific matrix composition, like ferrite. Similarly, this happens with silicon-alloyed steel without precipitated graphite,⁹ which in turn indicates that the effect is not based on conduction in graphite nodules. Precipitation out-of-solution as an explanation is also very unlikely in cast irons due to the non-supersaturating nature of silicon solution in iron. Carbon is also precipitated as graphite nodules or for example trapped in the matrix in the form of pearlite or other carbide compositions. In addition, normal cast iron chemical compositions contain very little

additional elements that can be considered to be alloying elements rather than minor trace occurrences from the production process or scrap material. There is also no indication of deviation from the general trend in Figure 1 when low cooling rates of ferritic and faster cooled pearlitic versions of the same alloys are concerned. The peak at an intermediate temperature for spheroidal graphite irons has been noted in studies and data gathered from multiple sources^{9,25} and is noted also in established literature on the matter,⁷ but is not really explained or not often even speculated upon in any meaningful manner. Definite conclusions cannot be drawn on the matter from the results and work in this study, but the findings suggest that the behavior is not exclusive to a certain microstructure rather than more a property of iron–silicon alloy system. Phonon contribution, also known as lattice vibration, could play a part in all this through thermal excitation behavior.

Increase in pearlite fraction decreases thermal conductivities in all tested alloys. The relation between microstructure and thermal conductivity shows as a linear decrease, illustrated in the effect plot in Figure 5. The phenomena behind the results can at least partly be accredited to hindering of conduction due to distortion of lattices with solution elements⁴ and the lamellar composite form of pearlite. Pearlite, being a composite form of ferrite and iron carbide, cementite (Fe_3C), has many interfaces and directions that hinder conduction along with the fact that cementite in general has poor conductivity.^{9,16,26} The general theory of thermal conduction in metallic materials states that the purer and more homogenous a crystal lattice is, the less disruption is imposed upon thermal energy carriers like electrons and phonons. In the case of cast irons, silicon is an element that forms a solid solution with iron matrix. Carbon is out-of-solution as precipitated graphite particles does not have such effects and has little effect on thermal properties due to its' morphology compared to graphite in compacted or flake form. If only good thermal conductivity is concerned in spheroidal graphite irons, low silicon ferritic matrix is the best choice and seems to even rival the conductive properties of some lamellar graphite cast irons.²⁵ The results in this work highlight the difference between ferritic–pearlitic grades and the newer silicon solution-strengthened ferritic (SSF) grades. The new GJS 500-14 and GJS 600-10 are used as direct replacements to ferritic–pearlitic grades, so these differences should be kept in mind. Mechanically, the new grades surpass the older ones by quite a wide margin,^{18–20} but thermal properties do not improve in the same way as seen from literature and the detailed results of this study. This in turn might create some unforeseen behavior if not taken into proper consideration in component design. Knowledge of true material behavior is thus of utmost importance as previously mentioned.

Conductivities estimated from the regression model ($R^2 = 0.92$) agree well with appropriate measured data.

The estimation also works well for a test material with added copper alloying. The addition of copper will influence microstructure through a pearlitizing effect, in addition to increasing the total alloying level. The results show that the model will give good estimations even on ferrite–pearlite microstructures that are controlled with alloying in small amounts, rather than with heat treatments. Naturally, a simple regression model cannot fully cover all aspects of complex composites such as graphitic cast irons. However, in the case of spheroidal graphite irons where large deviations in nodularity are unacceptable in production, these kinds of models that exclusively estimate properties through matrix behavior should work accurately. Modeling thermal conductivities of steels and cast irons have been made with various kinds of techniques ranging from microstructural approaches to composition analysis with artificial neural networks.^{14,16,27} These studies highlight a few important additional aspects, like the need for fundamental data on microstructural constituents and the complex effect of key alloying elements. For example, silicon studied in this work, is easy to account for being an element just in solid solution, not as a precipitating super-saturated element like in aluminum–silicon cast alloys. However, others like copper or tin do not have such straightforward interactions. Cast iron alloying and substitutive elements can act as pearlitizing, pearlite stabilizing, ferrite stabilizing, graphitizing and the like due to their more complex interactions in iron–carbon systems. Thus, taking a similar regression approach as taken in this study with a larger number of alloying elements as parameters without analyzing their final effect on things like microstructure, is a recipe for disaster.

Conclusion

Thermal conductivities of several spheroidal graphite cast iron alloys were studied with transient plane source measurement system. The main conclusion from this study are

- Increase in silicon alloying decreases thermal conductivity in all studied alloys. More silicon in solid solution makes ferrite less conductive, while it is known from other studies to increase mechanical properties. The effect of silicon on thermal conductivity is not linear. The change is more drastic in the lower alloying ranges and saturates at a higher level.
- Increase in pearlite in the microstructure decreases thermal conductivity in all studied alloys. Pearlite is a hindrance to thermal conduction due to its composition and lamellar form. The effect mirrors that of silicon alloying, although the effect is linear.
- Increase in temperature increases thermal conductivity of almost all samples until a peak is attained. A similar peak near 200–300 °C as found in this

study has also been noted in other research on the matter.

- Regression model for thermal conductivity is made, which agrees well with tests made with additional as-cast alloys. The model covers ferritic–pearlitic spheroidal graphite cast irons in the normal $\sim 1\text{--}4\%$ range of silicon alloying.

Acknowledgements

This study was made as part of the DIMECC (Digital, Internet, Materials & Engineering Co-Creation) project ‘Breakthrough steels and applications: Novel Cast Materials.’ Authors would like to thank Aalto University School of Engineering, Department of Mechanical Engineering for the facilities to conduct experiments. Funding was provided by Tekes.

REFERENCES

1. J. Olofsson, I.L. Svensson, *Mater. Des.* **34**, 494–500 (2012)
2. J. Olofsson, I.L. Svensson, *Mater. Des.* **43**, 264–271 (2013)
3. R. Cenni, M. Cova, G. Bertuzzi, *Proc. Inst. Mech. Eng. Part C*. 2016 03/29; 2017/01:0954406216640807
4. R.K. Williams, R.S. Graves, F.J. Weaver, D.W. Yarbrough, *J. Appl. Phys.* **62**(7), 2778–2783 (1987)
5. W.F. Gale, T.C. Totemeier (eds.), *Smithells Metals Reference Book*, 8th edn. (Elsevier, New York, 2004)
6. R.B. Gundlach, *Giesserei-Praxis*. **1–2**, 1–25 (1985)
7. E. Nechtelberger (ed.), *The Properties of Cast Iron up to 500 °C* (Verlag Schiele & Schön, Berlin, 1977)
8. M. Sasaki, K. Taniguchi, C. Yoshida, T. Sakamoto, *Trs. Jpn. Foundrym. Soc.* **4**, 37 (1985)
9. T. Okamoto, A. Kagawa, K. Kamei, H. Matsumoto, *J. Trans. Jpn. Foundrym. Soc.* **4**, 32–36 (1985)
10. D. Holmgren, A. Diószegi, I.L. Svensson, *Int. J. Cast Met. Res.* **20**(1), 30–40 (2007)
11. D.M. Holmgren, A. Diószegi, I.L. Svensson, *Int. J. Cast Met. Res.* **19**(6), 303–313 (2006)
12. D. Holmgren, R. Källbom, I.L. Svensson, *Metall. Mater. Trans. A*. **38**(2), 268–275 (2007)
13. D. Holmgren, A. Diószegi, I.L. Svensson, *Tsinghua Sci. Technol.* **13**(2), 170–176 (2008)
14. J.K. Chen, S.F. Chen, *InTech*. (2011)
15. D. Holmgren, I.L. Svensson, *Int. J. Cast Met. Res.* **18**(6), 321–330 (2005)
16. J. Helsing, G. Grimvall, *J. Appl. Phys.* **70**(3), 1198–1206 (1991)
17. H. Kempers, *Giesserei* **53**(1), 15–18 (1966)
18. R. Larker, *China Foundry*. **4**(12), 343–351 (2009)
19. H. Löblich, W. Stets, G. Gassner, P. Schumacher, *Giesserei*. **3**, 28–32 (2012)
20. W. Stets, H. Löblich, G. Gassner, P. Schumacher, *Int. J. Metalcast.* **8**(2), 35–40 (2014)
21. C. Cingi, V. Rauta, E. Suikkanen, J. Orkas, *Adv. Mater. Res.* **538–541**, 2047–2052 (2012)
22. M. Gustavsson, E. Karawacki, S.E. Gustafsson, *Rev. Sci. Instrum.* **65**(12), 3856–3859 (1994)
23. Y. He, *Thermochim. Acta* **436**, 122 (2005)
24. V. Rauta, C. Cingi, J. Orkas, *Int. J. Metalcast.* **10**(2), 157–171 (2016)
25. D. Holmgren, *Int. J. Cast Met. Res.* **18**(6), 331–345 (2005)
26. J.W. Donaldson, *Foundry Trade J.* **63**, 141–144 (1940)
27. M.J. Peet, H.S. Hasan, H.K.D.H. Bhadeshia, *Int. J. Heat Mass Transf.* **54**(11–12), 2602–2608 (2011)